New insights into thermomechanical behavior of GeTe thin films during crystallization

Marion Gallard, Mohamed Salah Amara, Magali Putero, Nelly Burle, Christophe Guichet, Stéphanie Escoubas, Marie-Ingrid Richard, Cristian Mocuta, Rebbeca R Chahine, Mathieu Bernard, et al.

New insights into thermomechanical behavior of GeTe thin films during crystallization

M. Gallard[1,2], M. S. Amara[1], M. Putero[1*], N. Burle[1], C. Guichet[1], S. Escoubas[1], M.-I. Richard[1,3], C. Mocuta[2], R. R. Chahine[4], M. Bernard[4], P. Kowalczyk[4], P. Noé[4], O. Thomas[1]

[1] Aix-Marseille Université, CNRS, IM2NP UMR 7334, Campus de St-Jérôme, 13397 Marseille Cedex 20, France
[2] Synchrotron SOLEIL, l'Orme des Merisiers, Saint-Aubin–BP 48, 91192 Gif-sur-Yvette, France
[3] ID01/ESRF, The European Synchrotron, 71 rue des Martyrs, 38043 Grenoble, France.
[4] Université Grenoble Alpes, CEA-LETI, MINATEC, 17 rue des Martyrs, 38054 Grenoble, France.

[*]Corresponding author: Magali Putero

Key-word: phase change materials, GeTe, chalcogenide, precipitation, stress, crystallization, sheet resistance, PCRAM

ABSTRACT

In this work, we reexamine Ge rejection in Ge-rich GeTe thin films with a slight deviation from stoichiometry using a unique combination of *in situ* measurements: curvature and x-ray diffraction as well as electrical resistance and x-ray diffraction and reflectivity during annealing. This unique combination of several experiments performed simultaneously on a synchrotron beamline allows to monitor *in situ*, during the crystallization and phase transformation, the microstructure, the strain and the stress changes, as well as electrical properties of GeTe films. Structural, electrical and thermomechanical evolutions of the GeTe thin films upon annealing are shown to follow three different steps. Stage I, before crystallization, is characterized by a tensile stress variation and a small decrease of the mass density. Stage II corresponds to the rhombohedral αGeTe phase crystallization leading to an abrupt tensile stress jump (+72 MPa), a mass density increase, and followed by a slight compressive stress evolution. During stage III, Ge crystallization is observed leading to a compressive stress jump (-54 MPa), an abrupt increase in αGeTe lattice spacing and diffracted intensity, whereas αGeTe diffraction peak widths decrease. During cooling a thermoelastic behavior is observed. A detailed analysis of stage III (Ge precipitation and crystallization) is performed and discussed regarding structural, stress, microstrain, electrical and thermomechanical properties. In particular, this study reveals that crystalline Ge precipitation results in important changes (volume of the unit cell, homogeneity of lattice spacing, average stress …) in the surrounding GeTe matrix. Different scenarios are proposed to understand these results.

1. Introduction

One of the leading materials for new emerging non-volatile memories are phase change materials (PCMs). PCMs have been successfully employed in optical memories such as DVD-RAM since the 1990s and more recently in the commercial production of electronic non-volatile phase-change random access memory (PCRAM)[1–3]. They are also deeply studied by academia for numerous new application and for the complex physics associated with their properties[4,5]. PCMs are characterized by a unique combination of properties[6] and continue to pose challenges for very basic fundamental research[7,8]. They exist in an amorphous and a crystalline phase with huge different optical and electrical properties caused by an unusual change of bonding when the amorphous phase is crystallized[8,9]. The amorphous phase exhibits in general high electrical resistivity and low optical reflectance, and the reverse properties are observed in the crystalline phase[10]. The capability to change the phase of such a material in very short times (nanoseconds) and repeatedly between the two phases makes PCMs ideal candidates for data storage. Among the large class of PCMs, the two prototypes and most studied materials are the $Ge_2Sb_2Te_5$ and GeTe chalcogenide alloys. They both belong to the GeTe–Sb_2Te_3 pseudo-binary diagram[11] and GeTe was one of the first binary alloy showing fast recrystallization and good optical contrast.

The Ge-enrichment of PCM alloys allows to stabilize the amorphous state resulting in a better thermal stability and data retention[12,13]. However, in such non-stoichiometric alloy, both the phase separation upon crystallization and the strain energy of crystallites nucleated in amorphous matrix have been shown to play a crucial role for PCRAM performances[14]. Ge segregation in Ge-rich alloys is for example at the origin of failure mechanisms in PCRAM devices[15,16]. Previous studies about Ge-enrichment in Ge-Sb, Ge-Te, and GeSbTe alloys have shown that the excess Ge always precipitates and crystallizes above the alloy crystallization temperature (T_x). In Ge-Sb alloy, Ge enrichment is shown to increase T_x[17], the crystallization of GeSb being followed by Ge precipitation and crystallization[18]. Even without Ge-enrichment, the annealing of as-deposited amorphous Ge_xSb_{1-x} alloy ($x < 0.4$) leads to Sb-rich phase crystallization followed by the formation of amorphous Ge regions that crystallize afterward, the Ge crystallization occurring thus at relatively low temperature[19,20]. In other systems such as Ge-rich GeSbTe or Ge-rich GaSb alloy[21], the precipitation and crystallization of pure Ge is also observed at temperatures slightly higher than T_x, Ge grains (~10nm) being embedded in the GeSbTe matrix[22]. Concerning Ge-rich Ge_xTe_{1-x} thin films (with $0.5 < x < 0.66$), the precipitation and crystallization of the excess element are usually observed[23] at a temperature larger than the crystallization temperature (T_x) of rhombohedral GeTe [3,16,24]. However, very few studies explain such Ge precipitation and crystallization at a temperature around 300°C, that is much lower than the Ge crystallization temperature[25]. Moreover the description of the crystallization process often suffer from a lack of accurate *in situ* measurements, most experimental studies producing *ex situ* analysis after annealing at different temperatures. In Ge-Sb alloys, previous studies[17,26] have discussed metal-induced crystallization as a possible mechanism for the Ge crystallization and precipitation: they describe a process that starts by crystallization and diffusion of Sb in a Ge–Sb matrix. Sb diffusion could induce Ge crystallization through Ge–Sb bond breaking comparable to a metal-induced crystallization process. In $Ge_{0.6}Te_{0.4}$, Yi et al.[27] have shown by *ab initio* molecular dynamics simulation that Ge atoms prefer to clump

together and form Ge tetrahedral clusters in the amorphous phase, possibly explaining experimental findings of segregation of crystalline Ge grains. In $Ge_{0.63}Te_{0.37}$ thin films, Carria et al.[28] have evidenced the presence of amorphous Ge precipitates at the initial stage of the crystallization, the GeTe crystalline grains subsequently acting as a seed for Ge crystallization. The Ge precipitates were shown to be nestled inside the GeTe grains with some aligned crystal orientation. In this study, the atomic interdiffusivity was also estimated near the crystallization temperature and Tellurium was shown to be likely the diffusing species.

In this work, we reexamine Ge rejection in Ge-rich GeTe thin films with a slight deviation from stoichiometry using unique combinations of *in situ* measurements: curvature and x-ray diffraction as well as electrical resistance and x-ray diffraction and reflectivity during annealing. This unique combination of both experiments performed simultaneously on a synchrotron beamline allows to monitor *in situ* during the crystallization and phase transformation the microstructure, the strain and the stress evolutions, as well as the electrical properties in thin PCM films[29]. Because of its peculiar sensitivity, this experimental *in situ* study gives new insights into the thermomechanical behavior of GeTe thin films during crystallization and Ge precipitation and the delicate interplay between composition and stress in these films.

2. Experimental procedures

100 nm thick GeTe film were deposited on 200 mm Si(001) substrates by magnetron sputtering from a nominally stoichiometric GeTe target. While for in situ X–ray reflectivity measurements 700 micron-thick substrates were used, 100 micron-thick silicon substrates were used for macroscopic curvature measurements to increase substrate bending under the film influence. The films were capped with 10 nm of TaN or SiN to prevent surface oxidation. After the deposition process, the film composition was assessed by means of Rutherford Backscattering Spectrometer (RBS) and Wavelength Dispersive X-ray Fluorescence (WDXRF), yielding slightly Ge-rich $Ge_{0.52\pm0.01}Te_{0.48\pm0.01}$ layers.

Samples were *in situ* annealed (2 °C/min) under nitrogen atmosphere in a chamber specially designed to simultaneously perform X-ray scattering (diffraction, XRD and/or reflectivity, XRR) and wafer curvature measurements[29,30]. The maximum annealing temperature was 400°C and the cooling rate was set to 5°C/min. The heating stage from Anton Paar® was equipped with a 300 µm thick PolyEtherEtherKetone (PEEK) dome for X-ray measurements and an optical quartz viewport to let the laser beam through for optical measurements of sample curvature. The furnace was mounted on the six-circle diffractometer (Kappa geometry) of the DiffAbs beamline at SOLEIL synchrotron. Square pieces of samples, about 10 × 10 mm^2 in size, were cut from the wafer and directly posed on the heating plate without clamping, so that they were free to bend during curvature measurements. The XRD patterns were recorded at a fixed grazing angle $\omega = 5°$ using a two-dimensional X-ray hybrid pixel array detector, XPAD[31,32]. An incident photon energy E = 16 keV or E = 18 keV was chosen in order to measure a large angular range and to optimize combined XRD and XRR measurements. The diffracted intensities as a function of the diffracted angles 2θ were obtained after 1D azimuthal integration and by applying geometrical corrections and background subtraction[33,34]. It is worth emphasizing that in these experimental conditions with scattering angle ranging (2θ) between 12 and

24° the diffracting plane normals lie between 1 and 7° from the surface normal. Hence the information accessed by diffraction (for ex. interplanar distances, grain sizes…) is basically along the normal to the film surface. The XRR patterns were recorded in θ-2θ geometry, with a point detector, in less than 1 minute. At each temperature, before performing XRR, the sample surface was automatically realigned in the X-ray beam (height and zero of the incidence angle). The data processing for XRR patterns to extract both film thickness and mass density is detailed in the Supplemental Material.

Simultaneously to the X-ray data acquisition, the substrate curvature was monitored to get insight into the film stress as detailed in Ref.[29,35]. This has been performed with a kSA® multi-beam optical sensor (MOS), which uses an array of parallel laser beams generated by a 658 nm wavelength laser beam crossing two parallel plates etalons. The sample surface, perpendicular to the incident laser beams, reflects these laser spots, which are captured by a charge-coupled detector. The MOS system is first calibrated with an optical flat mirror. The spacing between the spots reflected by the flat mirror is used as a reference. The deformation of the array after reflection from the sample allows determining the sample curvature along two directions:

$$\kappa = \frac{\cos\alpha}{2L}\ \frac{d-d_0}{d_0} \qquad (1)$$

where L and α are respectively the sample-to-detector (CCD camera) distance and the incident angle of the beam on the sample surface. d and d_0 are respectively the distance between the laser spots before and after reflection from the sample. Knowing the substrate thickness h_S and its biaxial modulus M_S the force per unit length applied by the film on the substrate can be deduced:

$$F = M_S \frac{{h_S}^2}{6}(\kappa - \kappa_o) \qquad (2)$$

where κ_0 is the curvature of the bare substrate surface. Formula (2) is called Stoney equation and is valid provided the film thickness is small enough as compared with the substrate thickness and that the substrate remains in the small deformation regime (bow should remain smaller than the substrate thickness). Both conditions are met in the samples investigated in this work. In the case of a homogeneous in-plane stress σ_f in the film of thickness h_f, the force per unit length F writes:

$$F = \sigma_f h_f \qquad (3)$$

In this work, we used as κ_0 in formula (2) the initial room-temperature curvature of the film-substrate system. Hence the force F is a relative force with respect to the initial situation, which includes bare substrate curvature and residual stress in the as-deposited film.

Simultaneous *in situ* XRD, XRR and sheet resistance (R_s) measurements were also performed using another dedicated vacuum chamber (10^{-5} mbar) equipped with a heating stage and an aligned 4-point probe sheet resistance set-up[10,36]. For such experiment, Si(100) substrates covered by an insulating 500 nm thick thermal SiO_2 layer were used. The heating chamber was mounted on the six-circle diffractometer of the DiffAbs beamline at SOLEIL synchrotron, and XRD, XRR and R_s were recorded during the sample annealing using same constant heating and cooling rate as previously described. Both XRD and XRR measurements were performed as described above; simultaneously to the collection of XRR and XRD data, the sheet resistance was measured: the current was supplied by a Keithley 6220 precision current source, while the voltage was measured using a Keithley 2182A nanovoltmeter, with the 4-point probes lying on the sample surface.

3. STABLE PHASES OF GeTe AND CRYSTALLOGRAPHY OF THE LOW TEMPERATURE α PHASE

According to the equilibrium phase diagram[37] $Ge_{1-x}Te_x$ crystallizes in three different structures under atmospheric pressure. The homogeneity domain at 703 K is 50.3 – 51.5 Te at%. At room temperature, the stable phase is rhombohedral αGeTe (R3m space group) on the Ge-rich side and orthorhombic γGeTe (SnS structure) on the Te-rich side. Above 640-700 K the stable phase is cubic βGeTe (Fm$\bar{3}$m, NaCl type). There are some controversies about the nature of this α–β transition whether it is a Peierls transition or an order-disorder transition[6]. βGeTe may also be stabilized at room temperature under high pressure[38]. It is reported that the dominant non-stoichiometric defects in αGeTe are double ionized vacancies on the Ge sublattice[37].

At room temperature, the rhombohedral primitive unit cell αGeTe has the following lattice parameters[39]: a_R = 0.4281 nm and α = 58.359°. It is often convenient to use a multiple (M=3) hexagonal unit cell whose lattice parameters are related to the rhombohedral cell parameters by:

$$a_H = 2a_R \sin(\alpha/2)$$

$$\text{and } c_H = a_R\sqrt{3 + 6\cos\alpha} \qquad (4)$$

respectively $a_R = \frac{1}{3}\sqrt{3a_H^2 + c_H^2}$ (5)

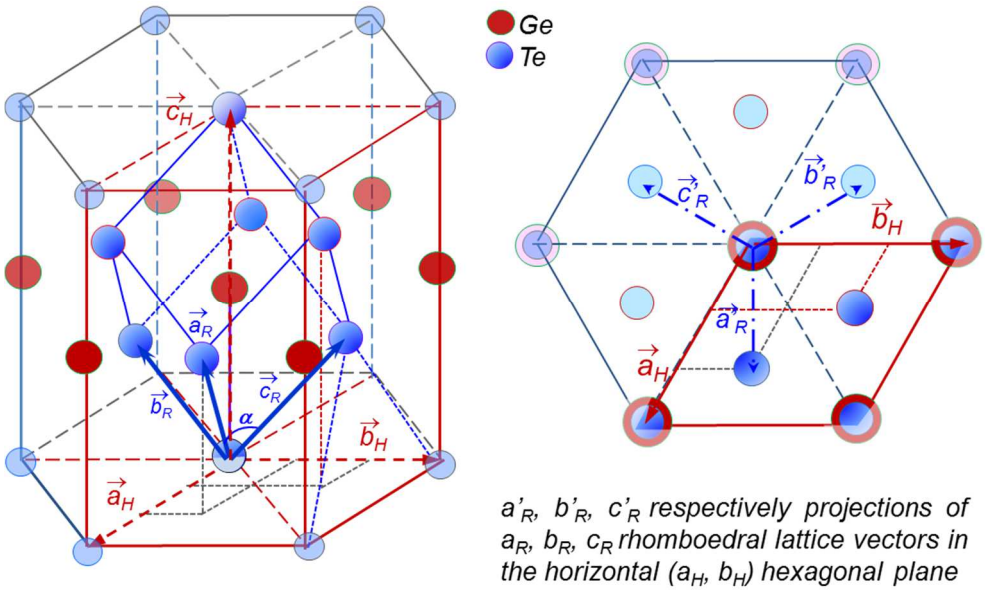

Figure 1 : Rhombohedric (in blue) versus hexagonal (in red) lattices; The basis is a Ge(0, 0, 0)-Te(0.475, 0.475, 0.475) pair in the rhombohedric cell, or Ge(0, 0, 0) – Te (0, 0, ½) in the hexagonal cell. Ge atoms are in blue; Te atoms are in red, for clarity not all of them are represented.

Hence the hexagonal parameters are a_H = 0.4174 nm ; c_H= 1.0614 nm (Fig.1). Slightly different values are reported by Chattopadhyay *et al.*[40]: a_H = 0.4164 nm ; c_H= 1.069 nm
In this article, the hexagonal simplest cell (M=3, in red in fig.1) is chosen to describe the lattice. As usual in the literature on GeTe, the three indices (*hkl*) notation is used (instead of (*h k i l*)).

It is worth noting that these αGeTe hexagonal lattice parameters yield very close interplanar distances for non-equivalent lattice planes: for example, (003)/(101), as well as (104)/(110) planes exhibit very similar interplanar distances (see Table 1). These small differences get even smaller when the temperature increases because of the anisotropic thermal expansion of αGeTe.

Thermal expansion of αGeTe has been measured by Chattopadhyay *et al.*[40] on single crystals. Using this data, one can extract the hexagonal thermal expansion coefficients α_a and α_c between 295 and 665 K: α_a= 3.19×10^{-5} K^{-1} and α_c = -2.05x10^{-5} K^{-1}. The volumetric thermal expansion is α_V = 4.33×10^{-5} K^{-1}, and the average linear thermal expansion coefficient is $\alpha_V/3$ = 1.44×10^{-5} K^{-1}. From temperature-dependent powder diffraction measurements[41], Chatterji reports α_V = 4.59×10^{-5} K^{-1}, which yields $\alpha_V/3$ = 1.53×10^{-5} K^{-1}. These measurements are in agreement with the earlier ones performed by Wiedemeier[42] and the most recent ones reported by Tran[43].

This high anisotropy in thermal expansion triggers the thermal evolution of lattice spacings. In the absence of stress, the thermal expansion of (*hkl*) lattice planes writes:

$$\alpha_{hkl} = \alpha_a - \left(\frac{a_0}{c_0}\right)^2 \frac{l^2}{\frac{4}{3}(h^2+k^2+hk)+\left(\frac{a_0}{c_0}\right)^2 l^2}(\alpha_a - \alpha_c) \quad (6)$$

The bulk modulus of GeTe has been measured by Onodera[38] as 49.9 GPa. The six independent elastic constants have been calculated within the density functional theory approximation[44,45]. The calculated extreme values of Young modulus show that R3m GeTe exhibits a strong elastic anisotropy: 48 GPa ≤ E ≤132 GPa[44] or 37 GPa ≤ E ≤ 119 GPa[45]. The softest direction is along the c-axis.

For the sake of completeness, it is worth mentioning the description of αGeTe with a pseudo-cubic unit cell, since the rhombohedral cell is very close to a cubic NaCl one, stretched along the <111> direction. The α–β transition may be then viewed as a pseudo-cubic to cubic transition. In that case the a_C parameter corresponds to the (111) interplanar distance of the primitive rhombohedral cell, which leads to a_C = 0.589 to 0.599 nm and α_C = 88.35 to 88.96° (instead of 90° in a cube).

4. Experimental results

Figure 2 shows the substrate curvature and XRD results obtained simultaneously *in situ* during annealing of a 100 nm GeTe film up to 400°C. On the right-hand side, XRD patterns (E = 16 keV) are shown as a function of temperature. The area detector was placed such that it covers in a single image a 2θ angular opening of about 5°; thus, two detector positions have been used yielding two 2θ ranges, from 12° to 16° and from 19° to 24° respectively. Starting from room temperature no diffraction peaks are visible, which is in agreement with the expected amorphous nature of as-deposited films. From

239°C on distinct diffraction peaks appear, that can be assigned to rhombohedral αGeTe. They are indexed accordingly (in the hexagonal description, see above) as 003/101, 012, and 104/110. This temperature is thus the crystallization temperature of GeTe noted T_x from now on. The value of T_x = 239°C is in good agreement with the literature for non-oxidized GeTe film[46]. Further heating makes faint additional peaks to appear at 297°C. These two additional peaks can be assigned to cubic Ge (diamond structure) and indexed as 111Ge and 220Ge. This temperature will be noted T_{Ge} from now on. In this combined experiment, $T_{Ge} \approx T_x + 58$°C, and $T_{Ge}/T_x \approx 1.25$. A clear displacement of αGeTe diffraction peaks is evidenced at T_{Ge}. Upon cooling no additional peaks appear but splitting of αGeTe 003/101 and 104/110 peaks is evidenced.

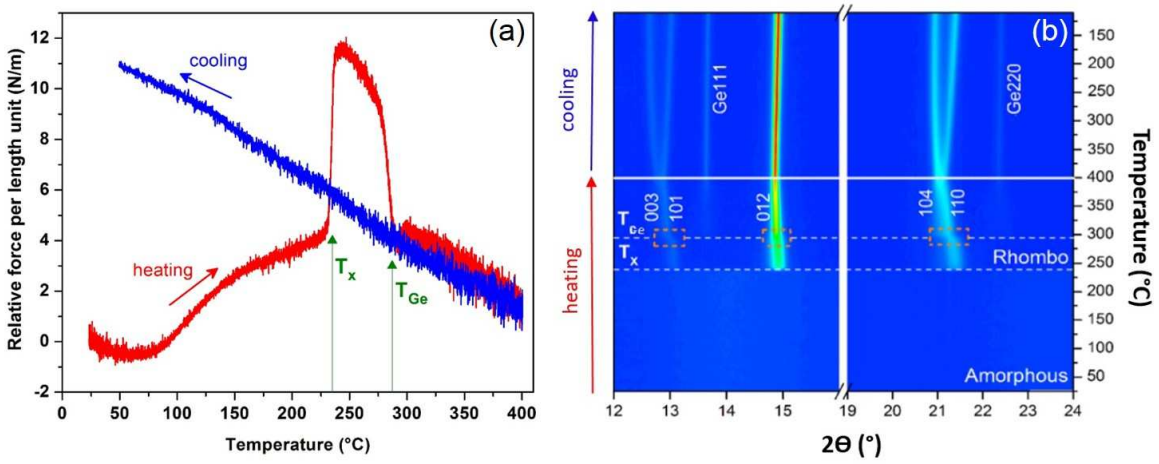

Figure 2 : In situ coupled measurements during the annealing of 100 nm GeTe films at 2°C/min. (a) Relative force deduced from substrate curvature; (b) XRD patterns (E=16 keV) as a function of temperature.

The force deduced from the sample curvature (equation 2) is plotted against temperature in the left-hand side of figure 2. Upon annealing, after a first compressive evolution up to 70°C, a smooth tensile stress buildup is then observed until T_x = 239°C where a sharp tensile increase happens. Further heating yields a smooth compressive trend followed by a sharp compressive drop at T_{Ge} = 297°C and a linear compressive trend. Cooling down translates into a linear tensile evolution. From the nominal 100 nm film thickness, one can deduce the stress jumps at T_x and T_{Ge} : +72 and -54 MPa respectively. These values are extracted assuming a constant thickness.

The diffraction peaks have been fitted using a Gaussian function and a linear background using a home-made python code. This allows extracting as a function of temperature the following parameters: peak integrated intensity, peak position and thus lattice spacing and peak width (FWHM).

The integrated intensity of αGeTe 012 and Ge 111 peaks is shown as a function of temperature in figure 3. At T_x a sharp increase of the 012 GeTe intensity is the signature of crystallization followed by a slow increase and a step at T_{Ge}. Upon cooling the intensity is almost constant with a slight increase that might be related to the Debye-Waller factor. The Ge 111 peak appears at T_{Ge} and steadily increases in intensity especially above 345°C (at ~T_{Ge}+50°C, or ~1.25T_{Ge}). The decreasing evolution of the integrated intensity of αGeTe 012 after T_{Ge} and upon cooling may be explained by the beginning of the GeTe rhombohedral-cubic phase transition (already shown to begin around

350°C[24]) for high temperatures and by the Debye-Waller effect for the lowest temperatures. However the indexation reported in Figures 2, 3 and 4 correspond to the hexagonal description of the rhomboedral α-GeTe phase. The characteristic splitting of the 003/101 and 104/110 peaks upon cooling is a fingerprint for this phase. Upon heating the breadth of the Bragg peaks does not allow for resolving these splittings but there are no signs for α–β phase transition, which should show up e.g. in the evolution of the peak widths.

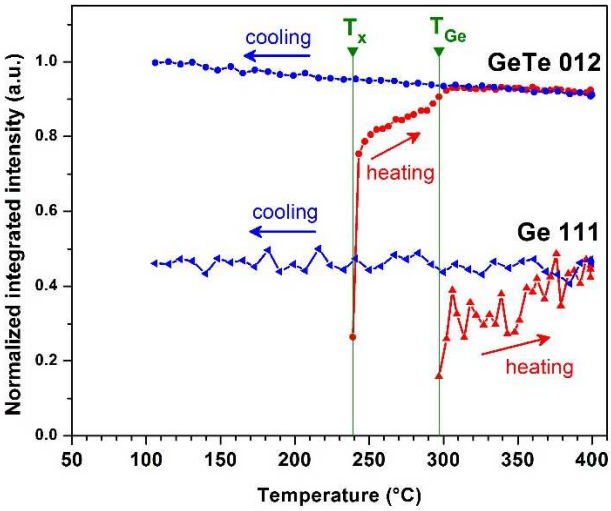

Figure 3 : Normalized integrated diffracted intensity of αGeTe 012 peak and Ge 111 peak. The normalization of the Ge 111 peak has been set to 0.5 for clarity. Its experimental integrated intensity is about 5 times smaller compared to GeTe 012.

Lattice spacings deduced from the peak positions are shown in figure 4. Above T_x, all spacings exhibit a positive thermal expansion behavior with a monotonous increase when the temperature rises. At T_{Ge}, a very distinct step is observed for all the measured spacings. Above T_{Ge}, positive thermal expansion resumes. Upon cooling specific splittings (003/101, 104/110) are observed with some peaks exhibiting negative thermal expansion in agreement with the reported thermal expansion coefficients[40–43]. Table 1 shows the calculated (eq.(6)) and measured values of thermal expansion coefficients α_{hkl} for the main (hkl) lattice planes of αGeTe phase: lattice planes having very close interplanar distances (*i.e.* 003/101, and 104/110) exhibit opposite thermal expansion coefficients, and the measured α_{hkl} are in very good agreement with the calculated ones, which implies very small thermoelastic strains in these supported films.

(hkl)	d_{hkl} (nm)	calculated α_{hkl} (K^{-1}) from eq.(6)	measured α_{hkl} (K^{-1}) from Fig.4
(003)	0.355 ± 0.002	-2.05×10^{-5}	-1.78×10^{-5}
(101)	0.342 ± 0.001	$+2.65\times10^{-5}$	$+3.26\times10^{-5}$
(012)	0.2988 ± 0.0005	$+1.53\times10^{-5}$	$+1.46\times10^{-5}$
(104)	0.2144 ± 0.0005	-0.22×10^{-5}	-0.14×10^{-5}
(110)	0.2084 ± 0.0005	$+3.19\times10^{-5}$	$+3.77\times10^{-5}$

Table 1: Temperature interplanar distances (at room temperature) and thermal expansion coefficients α_{hkl} for the main diffraction lines of αGeTe: theoretical α_{hkl} is calculated from eq. (6) and the lattice parameters from Ref.39 ; the measured α_{hkl} is calculated from the d_{hkl} of figure 4, during cooling, between 100°C and 300°C.

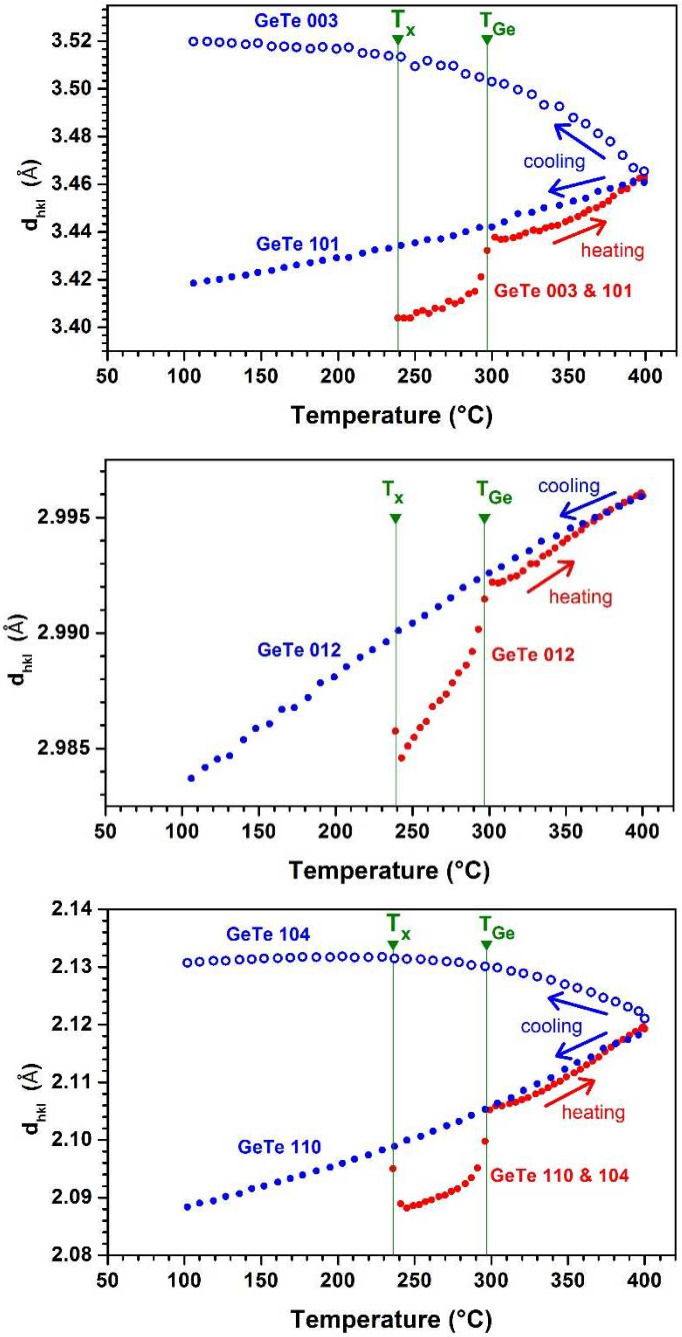

Figure 4: Lattice spacings in the αGeTe film as a function of temperature extracted from peak fitting of figure 2.

The thermal evolution of αGeTe 012 and Ge 111 FWHMs is shown in figure 5. Note that under experimental conditions, the experimental resolution on DiffAbs beamline is in the range of [0.04°-0.09°] in 2θ (and varying linearly with respect to the 2θ position of the XRD peak), leading to an experimental resolution around 2θ = 15° in reciprocal space units in the range of 0.07 nm^{-1}], thus

negligible in figure 5. The width of αGeTe 012 peak is decreasing with temperature with a sharp step down at T_{Ge}. Upon cooling this width stays constant. The width of Ge 111 peak decreases with annealing temperature and stays constant during the cooling stage.

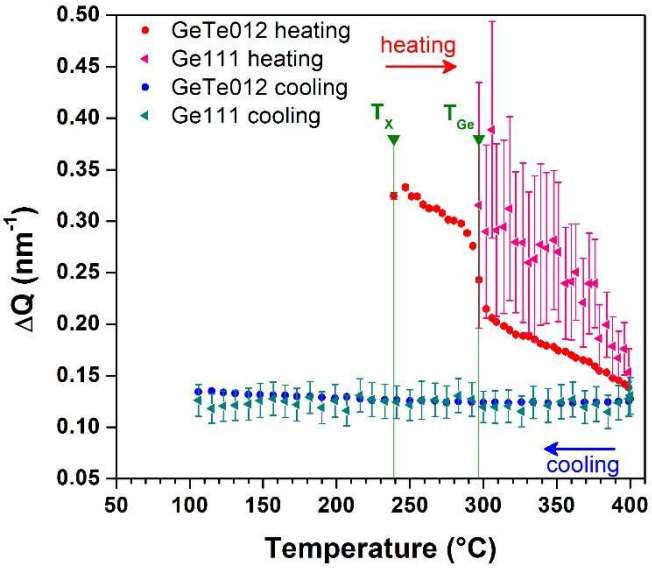

Figure 5: Diffraction peak widths of αGeTe 012 and Ge 111 as a function of temperature in reciprocal space units.

In-situ XRR patterns and total reflection edge (θ_c) variations are shown in figure 6 according to temperature. Starting from room temperature, the XRR patterns (total reflection edge θ_c and Kiessig fringes position) remain almost constant up to T_x where a clear shift in θ_c occurs towards higher angle (see figure 6b), corresponding to an increase in mass density. A second slight irregularity happens at T_{Ge}. During the heating stage, each XRR pattern was fitted to extract both the mass density and the film thickness change (see figure 7a). Figure 7b shows two XRR patterns recorded at the beginning of annealing (amorphous) and after T_x (crystallized), the corresponding fits, and a zoom on the total reflection edge indicating the shift through higher angle for the crystallized sample. Starting from a density of (5.64 ± 0.01) g.cm^{-3} and a film thickness of (98.8 ± 0.1) nm, these values show respectively an average decrease and increase of - 2.2 % and + 1.9 % even before reaching T_x. The average value of + 2% in the thickness variation up to T_x corresponds to a linear thermal expansion coefficient of ~2.2×10^{-5} K^{-1}, in good agreement with the average value of $\alpha_V/3$ reported in literature for crystalline GeTe [40–43]. Around T_x, the mass density and film thickness show respectively a relative variation of about + 8 % and - 7 %, then the mass density remains almost constant and the film thickness still changes to reach ~- 8 % at the end of annealing. From these data, the mass density of the GeTe film is calculated at 5.64 g/cm^3 and 6.07 g/cm^3 in respectively the amorphous and crystalized phases, corresponding to a relative variation of +7.6 %, in agreement with literature[39].

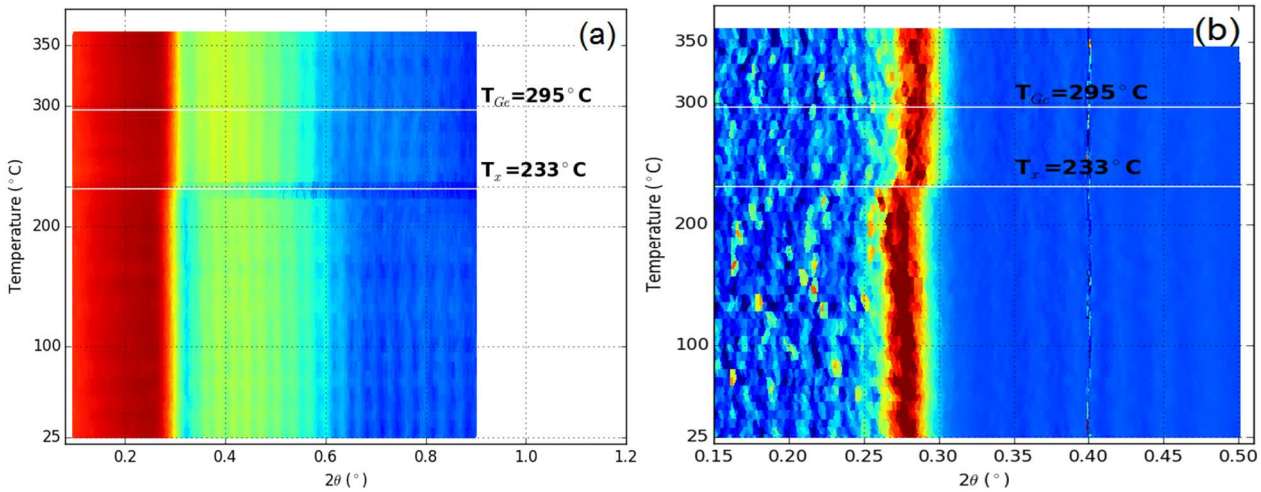

Figure 6: In situ combined XRR measurement (E = 18 keV) on 100 nm GeTe annealed at 2°C/min: (a) in situ XRR patterns; (b) Variation of the total reflection edge θ_c according to temperature (extracted from the derivative of XRR patterns).

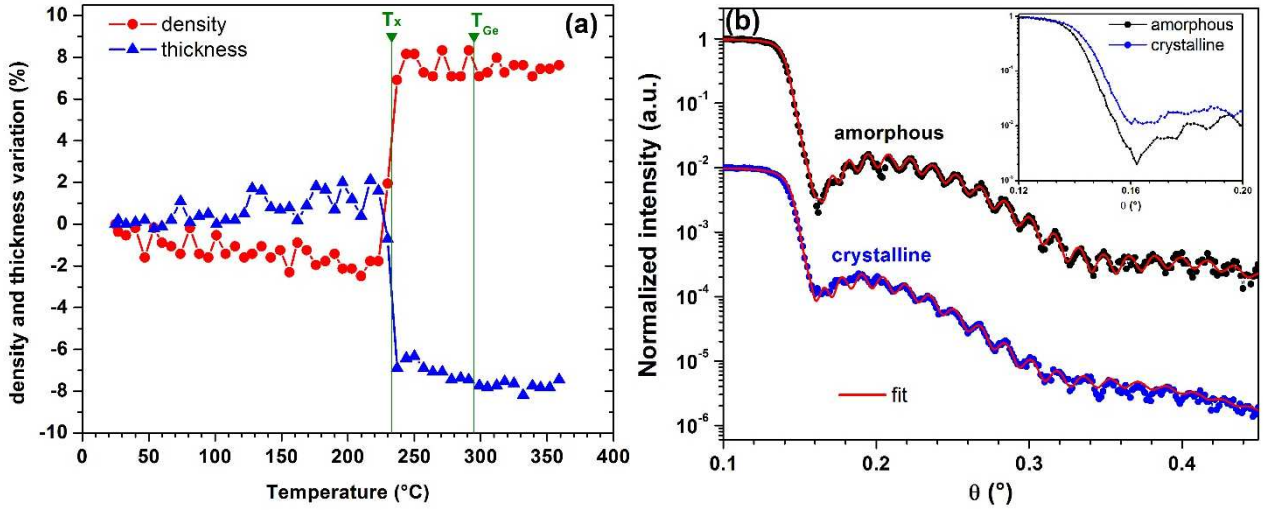

Figure 7: (a) Density and thickness relative variation extracted from the fit of in situ XRR patterns and (b) XRR experimental and fitted patterns recorded during annealing; as an example, 2 datasets are shown: at the beginning (amorphous sample) and at T = 339°C (crystalline sample).

Finally, to correlate the structural and electrical properties of the layer upon crystallization, combined XRD, XRR and R_s were performed. Figure 8a shows the evolution of R_s and XRD integrated intensity of αGeTe 012 and Ge 111 peaks with temperature upon *in situ* annealing up to 300°C and subsequent cooling. One should note that because of the sample holder pressing the sample on one side against the heating element, and because of the different thermal conditions compared to previous experiments (under vacuum *vs.* nitrogen atmosphere annealing), both T_x and T_{Ge} are shifted to lower temperatures; however, the data does not evidence any oxidation process responsible of such a shift[46], only the

different thermal conditions are involved. Apart from this shift in temperature, the XRD integrated intensity evolution shown in figure 8a are similar to the ones obtained in figures 2b and 3: actually, (i) the αGeTe 012 Bragg reflection shows a clear 2 step-growth (sharp increase at T_x followed by a slow increase and a step at T_{Ge}, with $T_{Ge} \approx T_x + 45°C$ and $T_{Ge}/T_x \approx 1.25$) and the same shift in 2θ position at T_{Ge}; and (ii) the Ge111 peaks displays a steady increase in intensity above 265°C (at ~T_{Ge}+45°C or ~1.2T_{Ge}). The sheet resistance evolution with temperature shows that the sample is initially in a highly resistive amorphous state, and, up to T_x, the resistance decreases with temperature as expected for a typical semiconductor. At T_x, the resistance drops suddenly by several orders of magnitude. A second drop of R_s occurs at T_{Ge}, then low resistance state is conserved upon cooling. Taking into account the film thickness at RT before and after crystallization, the resistivity is $\rho_a = 1.6 \times 10^3$ Ω.cm and $\rho_c = 1.05$ mΩ.cm, respectively in the amorphous and crystallized layer. The electrical contrast, defined as $\Delta R_S = \frac{R_{S\,before}}{R_{S\,after}}$, is 1.4×10^6. These values are all consistent with literature[47]. Both XRR (film thickness evolution) and XRD (GeTe 012 and Ge 111 integrated intensities) results are compared in figure 8b: the relative thickness variation is ~ 0.4 % before T_x (the corresponding linear thermal expansion coefficient is ~2.6 10^{-5} K^{-1}, thus in the same order of magnitude as in figure 7a), then a drastic decrease of -7.5 % occurs at T_x. At T_{Ge} a limited irregularity in the thickness evolution is visible. The relative variation of thickness after/before annealing is - 7.7 %, also in good accordance with previous results obtained with combined XRD and XRR only.

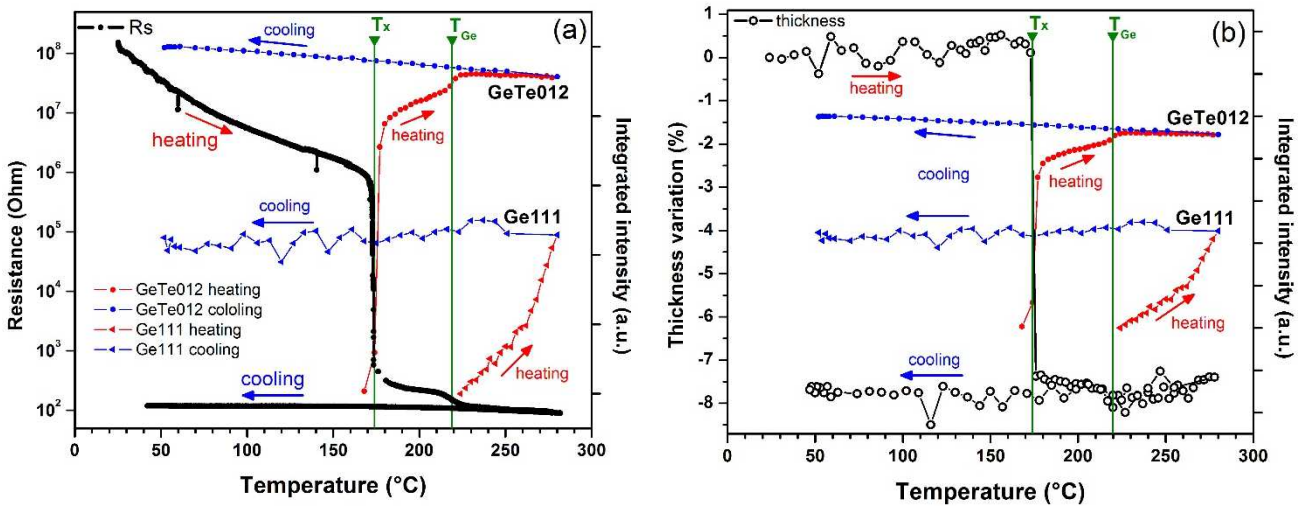

Figure 8: Results of combined XRD, XRR and R_s experiment on 100 nm GeTe layer capped with 10nm SiN. (a) R_s (left scale) and normalized integrated diffracted intensity (right scale) of αGeTe 012 peak and Ge 111 peak. The normalization of Ge 111 peak has been set to 0.5 for clarity. Its experimental integrated intensity is about 5 times smaller compared to GeTe 012. (b) relative layer thickness variation (left scale) deduced from XRR patterns and normalized integrated diffracted intensity (right scale) of αGeTe 012 peak and Ge 111 peak.

5. Discussion

The *in situ* evolutions during the annealing of the capped 100 nm GeTe films described in the previous section can be summarized in the following way:

- Stage I RT-T_x: Between room temperature and T_x= 239°C the film stays amorphous (no XRD peak), with a high electrical resistance state, and a tensile stress evolution is observed. During this stage a decrease of ~ - 2.2 % in mass density is measured by XRR, indicating that the tensile stress buildup is not related to a layer densification but rather to structural re-arrangements occurring in the amorphous GeTe phase during heating.
- Stage II T_x-T_{Ge}: at T_x=239°C an abrupt tensile stress jump is observed (+72 MPa) followed by a slight compressive stress evolution. αGeTe diffraction peaks appear at T_x as a consequence of crystallization. X-ray reflectivity indicates a densification of the film (+ 8 %) and a decrease of the film thickness (- 7 %). The electrical resistivity shows a decrease of several orders of magnitude.
- Stage III T_{Ge}- T_{max}: at T_{Ge}= 297°C diffraction peaks from Ge appear. At the same time distinct steps are observed in: (i) stress (compressive jump -54 MPa); (ii) αGeTe lattice spacings; (iii) αGeTe peak widths; (iv) αGeTe integrated intensity; (v) electrical resistivity (second decrease).
- Upon cooling the film stays crystallized. Both αGeTe and Ge diffraction peaks are present and exhibit a thermoelastic behavior.

Before focusing on stage III which shows the most novel results, a few points deserve to be highlighted concerning Stage II and crystallization. The crystallization temperature of our 100 nm thick GeTe films is 239°C, which shows that surface oxidation has been effectively prevented[46]. Crystallization is shown to be associated with an important increase in density together with a tensile stress buildup, in agreement with literature[48]. It is worth noting that such a density change should yield stresses of the order of several GPa if one takes into account the elastic constants of GeTe[44,45]. Although we do measure tensile stresses, in qualitative agreement with a densification, they are two orders of magnitude smaller than the ones predicted from elasticity. This shows that a very important relaxation of stresses occurs during crystallization, probably by viscous flow in the amorphous phase as already proposed in the literature[49].

Let us now discuss the interesting phenomena occurring upon Ge crystallization. In agreement with the initial film composition and with the equilibrium phase diagram[37], pure Ge precipitates within the film at T_{Ge}. Above T_{Ge} the decrease of the Ge111 peak width (Fig. 5) can be interpreted as an increase of the Ge grain size up to about 40 nm. The Ge 111 integrated intensity (Fig. 3 and 8), which is proportional to the amount of crystallized material in the absence of texture evolution, increases continuously as a function of temperature. Hence we observe both an increase in the quantity of crystallized Ge and an increase in grain size. *Post mortem* observations by atom probe tomography have recently evidenced large Ge grains in an annealed GeTe film[50]. As it is discussed in the introduction, excess Ge precipitation is rather common in thin chalcogenide films and has been described in several articles[18–23]. What has not been reported before are the consequences of this precipitation on the αGeTe phase. At T_{Ge}, a rather sharp increase in the GeTe lattice spacings is observed. From these spacings the average hexagonal lattice parameters are calculated and shown in

figure 9. Both a and c lattice parameters increase sharply at T_{Ge}, which translate in a 1.5 % increase in the volume of the unit cell. This volume increase agrees qualitatively with the compressive stress evolution evidenced by curvature measurements at T_{Ge}. Upon cooling one observes a negative thermal expansion coefficient along c, in agreement with literature[43]. Upon heating, the observed positive thermal expansion coefficient along c is probably related to the fact that both 003 and 101 diffraction lines, and 110 and 104 diffraction lines, are not resolved by the XRD measurement to be fitted separately, implying that only an average of the lattice spacings can be measured upon heating.

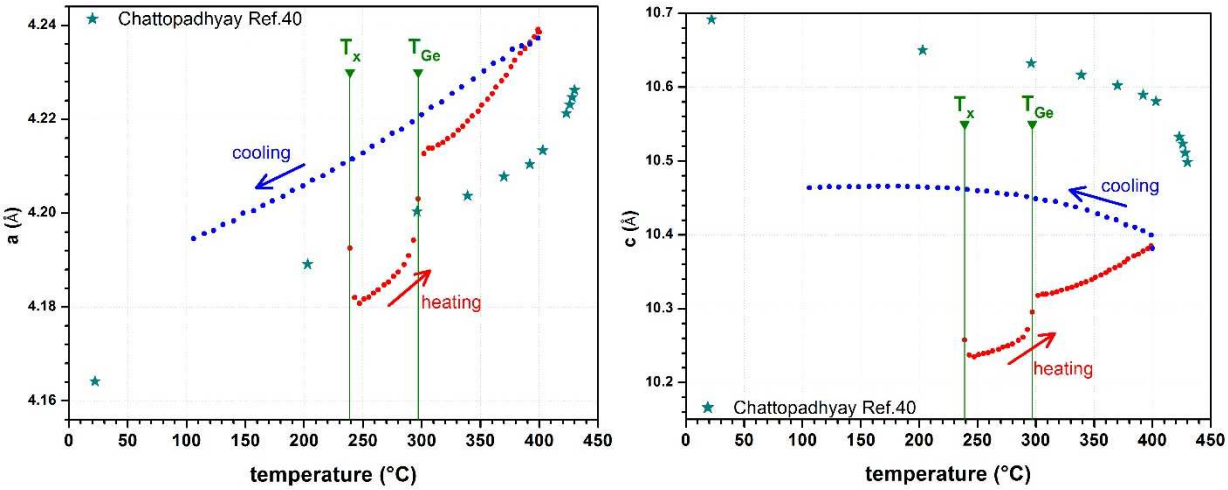

Figure 9: Lattice paramters of αGeTe as a function of temperature. Results from the literature on bulk samples [Ref.40] are also shown.

The width of the GeTe diffraction peaks (Fig. 5) shows a sharp drop at T_{Ge}. Although peak width is related to crystallite size (but not only), it is difficult to believe that GeTe grain size increases by 25% at T_{Ge} (Fig. 5). This drop is more likely caused by a sudden reduction of the dispersion in lattice spacing (inter grains or intra-grains). Such an effect is called microstrain in the line-profile-analysis community[51] and causes a peak broadening that is proportional to the distance to the origin of reciprocal space (whereas size broadening is independent on the position in reciprocal space). Without going to a very involved line profile analysis that is out of the scope of this study one can use a simple Williamson-Hall analysis[52], which states that size and micro-deformation broadening are additive:

$$\Delta q = 2\pi/L + \varepsilon\, q$$

where L is the crystal size, q the magnitude of the scattering vector and ε the microstrain, which is basically the standard deviation of the relative lattice spacing distribution. In the Williamson-Hall method one uses several orders of diffraction in order to plot Δq vs q and extract L and ε. Here we may assume that the step at T_{Ge} is purely caused by microstrains and that above T_{Ge} broadening is solely caused by size. Such a hypothesis yields: $\varepsilon = 5\text{x}10^{-3}$, an initial grain size of 26 nm (before T_{Ge}) and a final grain size of 40 nm (at T_{max}).

Finally, one may wonder about the state of Ge between T_x and T_{Ge}, *i.e.* when GeTe is crystallized and before the appearance of crystallized Ge. One may consider two extreme possibilities: 1) Ge is

in solution in αGeTe; 2) or Ge is an amorphous state. This makes two possible models for explaining our experimental findings.

- Model 1: Ge is in solid solution in αGeTe. At T_x, αGeTe crystallizes and excess Ge is within the unit cell in interstitial sites. At T_{Ge}, Ge becomes mobile and can precipitate out of the Ge-rich phase. In this interpretation, the volume of the unit cell needs to decrease upon Ge rejection. This decrease in volume in the supported film implies a compressive stress as observed experimentally. The increase of GeTe lattice parameters upon Ge rejection does not, however, agree with what has been published on the dependence of GeTe unit cell with composition: Hohnke[53] reports that the unit cell volume of Ge-saturated GeTe is larger than the one of Te-saturated GeTe. Diffracted intensity increase and resistivity decrease are related to the change in structure factor and doping respectively. The decrease in microstrain may be caused by an inhomogeneity in Ge excess concentration between grains below T_{Ge} that disappears when Ge is rejected leading to stable αGeTe.

- Model 2: An amorphous Ge shell is surrounding the αGeTe grains, with still small amorphous GeTe domains. It is actually worth noting that EXAFS analyses from Kolobov[54] seems to indicate the presence of amorphous Ge coexisting with crystallized GeTe. At T_x excess Ge is rejected in the form of a thin amorphous shell that surrounds the αGeTe grains and put them under compression. At T_{Ge}, Ge crystallizes in the form of localized grains thus relieving the applied stress, and leading to an increase in the GeTe unit cell volume. The remaining amorphous GeTe domains, having probably a Ge-rich composition, crystallize at the same temperature T_{Ge}, which is higher than T_x for stoichiometric GeTe, as already shown[24]. Diffracted intensity increase and resistivity decrease at T_{Ge} are related to the crystallization of remaining GeTe and/or to removal of amorphous Ge at GeTe grain boundaries that can be responsible for electronic localization effect and hindering thus electronic transport. The bulk modulus of αGeTe is of the order of 50 GPa hence the hydrostatic stress corresponding to 1.5% volume change is 750 MPa. This positive relief of internal strain in a supported film yields a compressive stress buildup, as observed. The disappearance of microstrains may be understood as a homogenization of the elastic strains in the film. Indeed at T_{Ge} the GeTe grains are not strained anymore by the amorphous Ge shell whereas below T_{Ge} elastic strains will vary from one grain to the other depending on the size and orientation of the grains as well as on the thickness of the shell. Moreover the disappearance of the amorphous Ge shell is likely to be responsible for the lowering of electrical resistance.

These two models are schematized in figure 10.

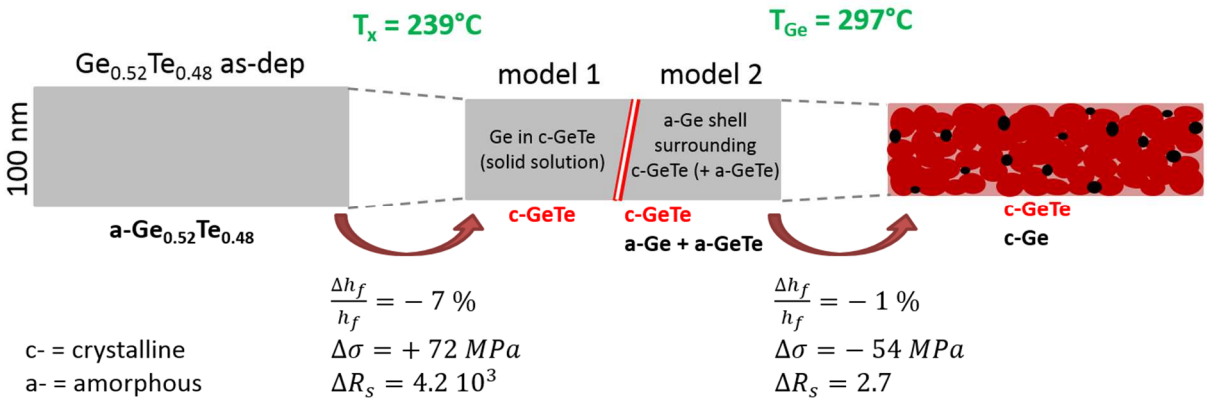

Figure 10: Schematic illustration of the two possible models. h_f is the layer thickness, σ is the stress, ΔR_s is the electrical contrast.

6. Conclusion

Original combinations of x-ray diffraction and x-ray reflectivity with curvature or resistance measurements have been performed *in situ* during annealing of initially amorphous GeTe thin films on silicon at DiffAbs beamline at SOLEIL synchrotron facility. These detailed experiments reveal a complex behavior with successive structural changes such as rhombohedral GeTe crystallization or cubic Ge precipitation accompanied by abrupt stress and resistance changes. In particular, this study reveals that crystalline Ge precipitation results in important changes (volume of the unit cell, homogeneity of lattice spacing, average stress, …) in the surrounding GeTe matrix. Different scenarios are proposed to understand these results. Future works at the local scale (atom probe tomography, transmission electron microscopy) will certainly help in selecting which scenario is at work. Based on our results we suggest, however, that the formation of an amorphous Ge shell around GeTe grains is the most probable event. Beyond its fundamental interest, this complex interplay between stress and composition in GeTe thin films has important implications for PCRAM technology. Indeed phase change materials used in Non-Volatile Memories are often strongly off-stoichiometric and Ge rejection and crystallization play a key role in the functioning of these devices.

ACKNOWLEDGMENTS

This work has been funded by ANR under contract SESAME ANR-15-CE24-0021. We would like to thank SOLEIL synchrotron for allocating beamtime on DiffAbs beamline.

Ph. Joly (Synchrotron SOLEIL, DiffAbs) is thanked for technical support.

REFERENCES

[1] V.L. Deringer, R. Dronskowski, M. Wuttig, Microscopic Complexity in Phase-Change Materials and its Role for Applications, Adv. Funct. Mater. 25 (2015) 6343–6359. doi:10.1002/adfm.201500826.

[2] G.W. Burr, M.J. BrightSky, A. Sebastian, H.-Y. Cheng, J.-Y. Wu, S. Kim, N.E. Sosa, N. Papandreou, H.-L. Lung, H. Pozidis, E. Eleftheriou, C.H. Lam, Recent Progress in Phase-Change Memory Technology, IEEE J. Emerg. Sel. Top. Circuits Syst. 6 (2016) 146–162. doi:10.1109/JETCAS.2016.2547718.

[3] P. Noé, C. Vallée, F. Hippert, F. Fillot, J.-Y. Raty, Phase-change materials for non-volatile memory devices: from technological challenges to materials science issues, Semicond. Sci. Technol. 33 (2018) 13002. doi:10.1088/1361-6641/aa7c25.

[4] A. Caretta, B. Casarin, P. Di Pietro, A. Perucchi, S. Lupi, V. Bragaglia, R. Calarco, F.R.L. Lange, M. Wuttig, F. Parmigiani, M. Malvestuto, Interband characterization and electronic transport control of nanoscaled GeTe/Sb2Te3 superlattices, Phys. Rev. B. 94 (2016) 045319. doi:10.1103/PhysRevB.94.045319.

[5] J.-J. Wang, Y.-Z. Xu, R. Mazzarello, M. Wuttig, W. Zhang, A Review on Disorder-Driven Metal–Insulator Transition in Crystalline Vacancy-Rich GeSbTe Phase-Change Materials, Materials (Basel). 10 (2017) 862. doi:10.3390/ma10080862.

[6] J.E. Boschker, R. Wang, R. Calarco, GeTe: A simple compound blessed with a plethora of properties, CrystEngComm. 19 (2017) 5324–5335. doi:10.1039/c7ce01040k.

[7] J.Y. Raty, W. Zhang, J. Luckas, C. Chen, R. Mazzarello, C. Bichara, M. Wuttig, Aging mechanisms in amorphous phase-change materials, Nat. Commun. 6 (2015) 1–8. doi:10.1038/ncomms8467.

[8] J. Raty, M. Schumacher, P. Golub, V.L. Deringer, C. Gatti, M. Wuttig, A Quantum-Mechanical Map for Bonding and Properties in Solids, Adv. Mater. 31 (2019) 1806280. doi:10.1002/adma.201806280.

[9] M. Wuttig, S. Raoux, The Science and Technology of Phase Change Materials, Zeitschrift Für Anorg. Und Allg. Chemie. 638 (2012) 2455–2465. doi:10.1002/zaac.201200448.

[10] M. Putero, T. Ouled-Khachroum, M.-V. Coulet, D. Deleruyelle, E. Ziegler, C. Muller, Evidence for correlated structural and electrical changes in a Ge 2 Sb 2 Te 5 thin film from combined synchrotron X-ray techniques and sheet resistance measurements during in situ thermal annealing, J. Appl. Crystallogr. 44 (2011) 858–864. doi:10.1107/S0021889811024095.

[11] N. Yamada, E. Ohno, N. Akahira, K. Nishiuchi, K. Nagata, M. Takao, High speed overwritable phase change optical disk material, Jpn. J. Appl. Phys. 26 (1987) 61–66.

[12] H.-Y. Cheng, J. Wu, R. Cheek, S. Raoux, M. BrightSky, D. Garbin, S. Kim, T. Hsu, Y. Zhu, E. Lai, E. Joseph, A. Schrott, S. Lai, A. Ray, H. Lung, C. Lam, A thermally robust phase change memory by engineering the Ge/N concentration in (Ge, N) x Sb y Te z phase change material, in: IEDM Tech. Dig. IEEE Int. Electron Devices Meet., 2012: pp. 31.1.1-31.1.4. doi:10.1109/IEDM.2012.6479141.

[13] A. Kiouseloglou, G. Navarro, V. Sousa, A. Persico, A. Roule, A. Cabrini, G. Torelli, S. Maitrejean, G. Reimbold, B. De Salvo, F. Clermidy, L. Perniola, A Novel Programming Technique to Boost Low-Resistance State Performance in Ge-Rich GST Phase Change Memory, IEEE Trans. Electron Devices. 61 (2014) 1246–1254.

[14] M. Chen, K.A. Rubin, R.W. Barton, Compound materials for reversible, phase-change optical data storage, Appl. Phys. Lett. 49 (1986) 502–504. doi:10.1063/1.97617.

[15] S. Yoon, K. Choi, N. Lee, S. Lee, Y. Park, B. Yu, Nanoscale observations of the operational failure for phase-change-type nonvolatile memory devices using Ge2Sb2Te5 chalcogenide thin films, Appl. Surf. Sci. 254 (2007) 316–320. doi:10.1016/j.apsusc.2007.07.098.

[16] G. Navarro, V. Sousa, a. Persico, N. Pashkov, a. Toffoli, J.-C. Bastien, L. Perniola, S. Maitrejean, a. Roule, P. Zuliani, R. Annunziata, B. De Salvo, Material engineering of

GexTe100−x compounds to improve phase-change memory performances, Solid. State. Electron. 89 (2013) 93–100. doi:10.1016/j.sse.2013.07.005.

[17] S. Raoux, C. Cabral, L. Krusin-Elbaum, J.L. Jordan-Sweet, K. Virwani, M. Hitzbleck, M. Salinga, A. Madan, T.L. Pinto, Phase transitions in Ge–Sb phase change materials, J. Appl. Phys. 105 (2009) 064918. doi:10.1063/1.3091271.

[18] L. Krusin-Elbaum, D. Shakhvorostov, C. Cabral, S. Raoux, J.L. Jordan-Sweet, Irreversible altering of crystalline phase of phase-change Ge–Sb thin films, Appl. Phys. Lett. 96 (2010) 121906. doi:10.1063/1.3361656.

[19] G.B. Kim, J.H. Bae, S.M. Jeong, S.M. Choi, H.L. Lee, Crystallization properties of Ge1-xSbx thin films (x = 0.58-0.88, Jpn. J. Appl. Phys. 50 (2011). doi:10.1143/JJAP.50.045805.

[20] P. Zalden, G. Aquilanti, C. Prestipino, O. Mathon, B. André, M. Wuttig, M.V. Coulet, Simultaneous calorimetric and quick-EXAFS measurements to study the crystallization process in phase-change materials., J. Synchrotron Radiat. 19 (2012) 806–13. doi:10.1107/S090904951202612X.

[21] M. Putero, M.-V. Coulet, C. Muller, C. Baethz, S. Raoux, H.-Y. Cheng, Ge-doped GaSb thin films with zero mass density change upon crystallization for applications in phase change memories, Appl. Phys. Lett. 108 (2016) 101909. doi:10.1063/1.4943788.

[22] S.M.S. Privitera, V. Sousa, C. Bongiorno, G. Navarro, C. Sabbione, E. Carria, E. Rimini, Atomic diffusion in laser irradiated Ge rich GeSbTe thin films for phase change memory applications, J. Phys. D. Appl. Phys. 51 (2018). doi:10.1088/1361-6463/aab1d0.

[23] E. Gourvest, S. Lhostis, J. Kreisel, M. Armand, S. Maitrejean, A. Roule, C. Valĺe, Evidence of Germanium precipitation in phase-change Ge1-xTexthin films by Raman scattering, Appl. Phys. Lett. 95 (2009) 4–6. doi:10.1063/1.3186077.

[24] S. Raoux, B. Muñoz, H.-Y. Cheng, J.L. Jordan-Sweet, Phase transitions in Ge–Te phase change materials studied by time-resolved x-ray diffraction, Appl. Phys. Lett. 95 (2009) 143118. doi:10.1063/1.3236786.

[25] W. Knaepen, S. Gaudet, C. Detavernier, R.L. Van Meirhaeghe, J. Jordan-Sweet, C. Lavoie, In situ x-ray diffraction study of metal induced crystallization of amorphous germanium, J. Appl. Phys. 105 (2009) 83532. doi:10.1063/1.3110722.

[26] J.M. del Pozo, M.P. Herrero, L. Díaz, Crystallization behaviour of amorphous Ge(1 - x)Sbxthin films, J. Non. Cryst. Solids. 185 (1995) 183–190. doi:10.1016/0022-3093(95)00663-X.

[27] X. Yi, Z. Wang, F. Dong, S. Cheng, J. Wang, C. Liu, J. Li, S. Wang, T. Yang, W.S. Su, L. Chen, Structural and optical properties of Ge60Te40: Experimental and theoretical verification, J. Phys. D. Appl. Phys. 49 (2016) 155105. doi:10.1088/0022-3727/49/15/155105.

[28] E. Carria, A.M. Mio, S. Gibilisco, M. Miritello, C. Bongiorno, M.G. Grimaldi, E. Rimini, Amorphous-Crystal Phase Transitions in GexTe1-x Alloys, J. Electrochem. Soc. 159 (2012) H130. doi:10.1149/2.048202jes.

[29] T.O. Khachroum, M.-I. Richard, P. Noe, C. Guichet, C. Mocuta, C. Sabbione, F. Hippert, O. Thomas, Stress buildup during crystallization of thin chalcogenide films for memory applications: in situ combination of synchrotron X-Ray diffraction and wafer curvature measurements, Thin Solid Films. 617 (2016) 44–47. doi:10.1016/j.tsf.2016.02.020.

[30] C. Mocuta, S. Stanescu, M. Gallard, A. Barbier, A. Dawiec, B. Kedjar, N. Leclercq, D. Thiaudiere, Fast X-ray reflectivity measurements using an X-ray pixel area detector at the DiffAbs beamline, Synchrotron SOLEIL, J. Synchrotron Radiat. 25 (2018) 204–213. doi:10.1107/S1600577517015703.

[31] S. Basolo, J. Berar, N. Boudet, P. Breugnon, B. Caillot, J.-C. Clemens, P. Delpierre, B. Dinkespiler, I. Koudobine, C. Meessen, M. Menouni, C. Mouget, P. Pangaud, R. Potheau, E. Vigeolas, XPAD: Pixel detector for material sciences, 2005. doi:10.1109/TNS.2005.856818.

[32] P. Pangaud, S. Basolo, N. Boudet, J.F. Berar, B. Chantepie, J.C. Clemens, P. Delpierre, B. Dinkespiler, K. Medjoubi, S. Hustache, M. Menouni, C. Morel, XPAD3-S: A fast hybrid pixel readout chip for X-ray synchrotron facilities, Nucl. Instruments Methods Phys. Res. Sect. A

Accel. Spectrometers, Detect. Assoc. Equip. 591 (2008) 159–162. doi:10.1016/j.nima.2008.03.047.

[33] C. Le Bourlot, P. Landois, S. Djaziri, P.O. Renault, E. Le Bourhis, P. Goudeau, M. Pinault, M. Mayne-Lhermite, B. Bacroix, D. Faurie, O. Castelnau, P. Launois, S. Rouzire, Synchrotron X-ray diffraction experiments with a prototype hybrid pixel detector, J. Appl. Crystallogr. 45 (2012) 38–47. doi:10.1107/S0021889811049107.

[34] C. Mocuta, M.I. Richard, J. Fouet, S. Stanescu, A. Barbier, C. Guichet, O. Thomas, S. Hustache, A. V. Zozulya, D. Thiaudière, Erratum: Fast pole figure acquisition using area detectors at the DiffAbs beamline - Synchrotron SOLEIL (Journal of Applied Crystallography (2013) 46 (1842-1853)), J. Appl. Crystallogr. 47 (2014) 482. doi:10.1107/S1600576713032081.

[35] C. Rivero, P. Gergaud, M. Gailhanou, O. Thomas, B. Froment, H. Jaouen, V. Carron, Combined synchrotron x-ray diffraction and wafer curvature measurements during Ni–Si reactive film formation, Appl. Phys. Lett. 87 (2005) 041904. doi:10.1063/1.1999021.

[36] M. Putero, B. Duployer, I. Blum, T. Ouled-Khachroum, M.-V. Coulet, C. Perrin, E. Ziegler, C. Muller, D. Mangelinck, Combined in situ x-ray scattering and electrical measurements for characterizing phase transformations in nanometric functional films, Thin Solid Films. 541 (2013) 21–27. doi:10.1016/j.tsf.2012.11.131.

[37] D.I. Bletskan, PHASE EQUILIBRIUM IN BINARY SYSTEMS A 1 vBv 1, J. Ovonic Res. I (2005) 53–60.

[38] A. Onodera, I. Sakamoto, Y. Fujii, N. Môri, S. Sugai, Structural and electrical properties of GeSe and GeTe at high pressure, Phys. Rev. B. 56 (1997) 7935–7941. doi:10.1103/PhysRevB.56.7935.

[39] T. Nonaka, Crystal structure of GeTe and Ge2Sb2Te5 meta-stable phase, Thin Solid Films. 370 (2000) 258–261. doi:10.1016/S0040-6090(99)01090-1.

[40] T. Chattopadhyay, J.X. Boucherle, H.G. von Schnering, Neutron diffraction study on the structural phase transition in gete, J. Phys. C Solid State Phys. 20 (1987) 1431–1440. doi:10.1088/0022-3719/20/10/012.

[41] T. Chatterji, C.M.N. Kumar, U.D. Wdowik, Anomalous temperature-induced volume contraction in GeTe, Phys. Rev. B. 91 (2015) 054110. doi:10.1103/PhysRevB.91.054110.

[42] H. Wiedemeier, P.A. Siemers, The Thermal Expansion of GeS and GeTe, ZAAC - J. Inorg. Gen. Chem. 431 (1977) 299–304. doi:10.1002/zaac.19774310134.

[43] X.Q. Tran, M. Hong, H. Maeno, Y. Kawami, T. Toriyama, K. Jack, Z.G. Chen, J. Zou, S. Matsumura, M.S. Dargusch, Real-time observation of the thermally-induced phase transformation in GeTe and its thermal expansion properties, Acta Mater. 165 (2019) 327–335. doi:10.1016/j.actamat.2018.11.059.

[44] R. Shaltaf, E. Durgun, J.-Y. Raty, P. Ghosez, X. Gonze, Dynamical, dielectric, and elastic properties of GeTe investigated with first-principles density functional theory, Phys. Rev. B - Condens. Matter Mater. Phys. 78 (2008) 205203. doi:10.1103/PhysRevB.78.205203.

[45] H.L. Kagdada, P.K. Jha, P. Śpiewak, K.J. Kurzydłowski, Structural stability, dynamical stability, thermoelectric properties, and elastic properties of GeTe at high pressure, Phys. Rev. B. 97 (2018) 134105. doi:10.1103/PhysRevB.97.134105.

[46] R. Berthier, N. Bernier, D. Cooper, C. Sabbione, F. Hippert, P. Noé, *In situ* observation of the impact of surface oxidation on the crystallization mechanism of GeTe phase-change thin films by scanning transmission electron microscopy, J. Appl. Phys. 122 (2017) 115304. doi:10.1063/1.5002637.

[47] P. Jost, H. Volker, A. Poitz, C. Poltorak, P. Zalden, T. Schäfer, F.R.L. Lange, R.M. Schmidt, B. Holländer, M.R. Wirtssohn, M. Wuttig, Disorder-Induced Localization in Crystalline Pseudo-Binary GeTe-Sb2Te3 Alloys between Ge3Sb2Te6 and GeTe, Adv. Funct. Mater. 25 (2015) 6399–6406. doi:10.1002/adfm.201500848.

[48] K.N. Chen, C. Cabral, L. Krusin-Elbaum, Thermal stress effects of Ge2Sb2Te5 phase change

material: Irreversible modification with Ti adhesion layers and segregation of Te, Microelectron. Eng. 85 (2008) 2346–2349. doi:10.1016/j.mee.2008.09.009.

[49] J. Kalb, F. Spaepen, T.P.L. Pedersen, M. Wuttig, Viscosity and elastic constants of thin films of amorphous Te alloys used for optical data storage Viscosity and elastic constants of thin films of amorphous Te alloys used for optical data storage, J. Appl. Phys. 94 (2003) 4908. doi:10.1063/1.1610775.

[50] M. Zhu, O. Cojocaru-Mirédin, A.M. Mio, J. Keutgen, M. Küpers, Y. Yu, J.Y. Cho, R. Dronskowski, M. Wuttig, Unique Bond Breaking in Crystalline Phase Change Materials and the Quest for Metavalent Bonding, Adv. Mater. 1706735 (2018) 1–9. doi:10.1002/adma.201706735.

[51] E. J. Mittemeijer, P. Scardi, Diffraction analysis of the microstructure of materials, Springer Science & Business Media, 2003. doi:10.1007/978-3-662-06723-9.

[52] G.K. Williamson, W.H. Hall, X-RAY LINE BROADENING FROM FILED ALUMINIUM AND WOLFRAM, Acta Mettalurgica. 1 (1953) 22–31. doi:https://doi.org/10.1016/0001-6160(53)90006-6.

[53] D.K. Hohnke, H. Holloway, S. Kaiser, PHASE RELATIONS AND TRANSFORMATIONS IN THE SYSTEM PbTe-GeTe, J. Phys. Chem. Solids. 33 (1972) 2053–2062.

[54] A. V. Kolobov, J. Tominaga, P. Fons, T. Uruga, Local structure of crystallized GeTe films, Appl. Phys. Lett. 82 (2003) 382–384. doi:10.1063/1.1539926.

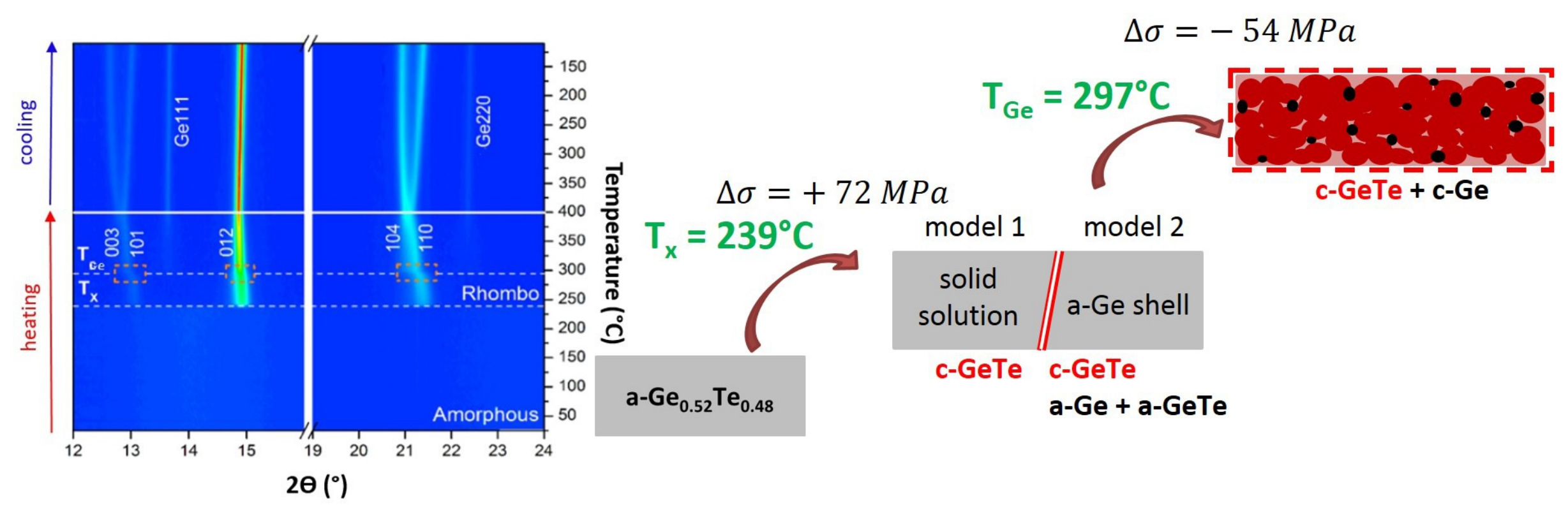
cooling
heating
Ge111
Ge220
003
101
012
104
110
T_{Ge}
T_x
Rhombo
Amorphous
12
13
14
15
19
20
21
22
23
24
2Θ (°)
150
200
250
300
350
400
350
300
250
200
150
100
50
Temperature (°C)
$\Delta\sigma = -54\ MPa$
T_{Ge} = 297°C
c-GeTe + c-Ge
$\Delta\sigma = +72\ MPa$
T_x = 239°C
model 1
model 2
solid solution
a-Ge shell
c-GeTe
c-GeTe
a-Ge + a-GeTe
a-$Ge_{0.52}Te_{0.48}$